Contribution from the Departments of Chemistry and Physics and Materials Research Center, Northwestern University, Evanston, Illinois 60208, and Centre de Recherche en Physique du Solide, Département de Physique, Université de Sherbrooke, Sherbrooke, Quebec J1K 2R1, Canada

Preparation, Characterization, and Low-Temperature Transition of Cu(tatbp)I, a New Porphyrinic Conductor with Local Moments Coupled to Itinerant Charge Carriers

Kwangkyoung Liou,[†] Michael Y. Ogawa,[†] Timothy P. Newcomb,[†] Guy Quirion,[‡] Moohee Lee,[§] Mario Poirier,*[,‡] William P. Halperin,*[,§] Brian M. Hoffman,*[,†] and James A. Ibers*[,†]

Received March 3, 1989

We present the preparation and characterization of a new metallomacrocycle-based molecular conductor, (triazatetrabenzoporphyrinato)copper(II) iodide, Cu(tatbp)I. The material crystallizes with two formula units in space group D_{4h}^2-$P4/mcc$ of the tetragonal system in a cell of dimensions a = 13.998 (5) Å and c = 6.426 (3) Å (120 K). The structure has been refined to a value of $R(F^2)$ of 0.085 for 862 data and 65 variables. This material is isostructural with (phthalocyaninato)copper(II) iodide, Cu(pc)I, and has analogous physical properties. However, Cu(tatbp) exhibits subtle metrical and electronic differences from Cu(pc) because the tatbp macrocycle has a methine carbon in place of one bridging nitrogen atom of pc. These differences produce distinct charge-transport and magnetic properties for each of the iodinated compounds. Cu(tatbp)I is a ring-oxidized organic conductor with metallic behavior that contains a dense array of localized Cu^{2+} moments embedded in the "Fermi sea" of carriers. ^{13}C NMR spectroscopy at 13 MHz of enriched and natural-abundance ^{13}C nuclei in Cu(tatbp)I show a distribution of positive and negative spin densities. The temperature dependence of the shifts identifies their origin as an isotropic contact hyperfine interaction transferred from Cu(II). EPR and magnetic susceptibility measurements show that the local and itinerant spin systems are coupled and that the local moments are exchange-coupled to one another by direct and carrier-mediated mechanisms. This unusual situation results in two novel transitions of the coupled systems: for $T < T_a \approx 20$ K, $g_\parallel$ increases anomalously as T is decreased; for $T < T_b \approx 6$–8 K the EPR line width begins to broaden sharply, but the signal of Cu(tatbp)I remains detectable to $T < 2$ K. Comparisons of X-band and Q-band data show that $g_\parallel$ is dependent on magnetic field at liquid-helium temperatures. Magnetic moments localized on the Cu^{2+} metal spine of Cu(tatbp)I also have a dramatic effect on the conductivity and dielectric constant. From ~90 to ≤10 K, both four-probe (27 Hz) and microwave (13 GHz) conductivities decrease by 3 orders of magnitude and both slightly increase with magnetic field. For $T < 6$ K the microwave conductivity is enhanced in comparison to the four-probe conductivity and decreases with field; over the same range the dielectric constant increases with field. These effects correlate with a relaxation of the local moments observed in EPR spectroscopy and reflect a dielectric loss associated with an unusual coupling between magnetic and dielectric properties.

Introduction

Highly conducting molecular crystals prepared from metallomacrocycle complexes comprise a class of conductors whose physical properties may be significantly altered by small modifications of their molecular subunits.[1-5] The first of these materials to be studied was (phthalocyaninato)nickel(II) iodide, Ni(pc)I.[5,6] This material consists of metal-over-metal stacks of partially oxidized metallomacrocycles surrounded by linear chains of I_3^- ions. Its charge carriers belong to the π molecular orbitals of the pc ring. Ni(pc)I is the first low-temperature molecular conductor that does not contain chalcogen atoms. A novel situation is created when the metal centers of Ni(pc)I are replaced by paramagnetic Cu^{2+} ions. In a previous paper[1] it was shown that Cu(pc)I exists as an organic conductor, that its intrinsically paramagnetic Cu^{2+} sites are exchange-coupled to one another by both direct and carrier-mediated mechanisms, and that the Cu^{2+} spin system is further coupled to the carrier spins. This unusual situation results in the occurrence of a new type of low-temperature transition characterized by an abrupt broadening and loss of the EPR signal of Cu(pc)I without an associated loss of paramagnetism.

The present work describes the preparation and characterization of the new metallomacrocycle-based molecular conductor (triazatetrabenzoporphyrinato)copper(II) iodide, Cu(tatbp)I

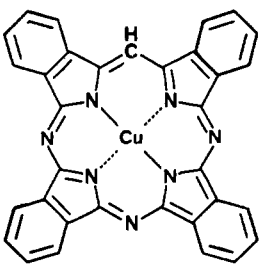

(the iodine atom is not shown). This material is isostructural with Cu(pc)I but differs from it by the substitution of a methine carbon for one bridging nitrogen atom of the ligand. We show here that Cu(tatbp)I, as well as Cu(pc)I, is a ring-oxidized organic conductor with partially oxidized Cu(tatbp) stacks that contain a dense one-dimensional array of localized Cu^{2+} moments. In addition to low-temperature transitions related to those seen in Cu(pc)I, we report effects of the local moments on the charge transport of Cu(tatbp)I as seen in comparisons between the four-probe and microwave conductivities (13 GHz).[3] The effects of Cu^{2+} spins on charge transport and on the dielectric constant are discussed in terms of magnetic scattering of the carriers as well as dielectric loss that results from a coupling between dielectric and magnetic properties.

Experimental Section

Synthesis. Triazatetrabenzoporphyrin, H_2(tatbp), was prepared as described in the literature.[7] H_2(tatbp) ^{13}C enriched at the methine

[†] Department of Chemistry, Northwestern University.
[‡] Université de Sherbrooke.
[§] Department of Physics, Northwestern University.

(1) (a) Ogawa, M. Y.; Martinsen, J.; Palmer, S. M.; Stanton, J. L.; Tanaka, J.; Green, R. L.; Hoffman, B. M.; Ibers, J. A. *J. Am. Chem. Soc.* **1987**, *109*, 1115–1121. (b) Ogawa, M. Y.; Hoffman, B. M.; Lee, S.; Yudkowsky, M.; Halperin, W. P. *Phys. Rev. Lett.* **1986**, *57*, 1177–1180.
(2) Pace, L. J.; Martinsen, J.; Ulman, A.; Hoffman, B. M.; Ibers, J. A. *J. Am. Chem. Soc.* **1983**, *105*, 2612–2620.
(3) (a) Quirion, G.; Poirier, M.; Ogawa, M. Y.; Hoffman, B. M. *Solid State Commun.* **1987**, *64*, 613–616. (b) Quirion, G.; Poirier, M.; Liou, K. K.; Ogawa, M. Y.; Hoffman, B. M. *Phys. Rev. B* **1988**, *37*, 4272–4275.
(4) Martinsen, J.; Stanton, J. L.; Greene, R. L.; Tanaka, J.; Hoffman, B. M.; Ibers, J. A. *J. Am. Chem. Soc.* **1985**, *107*, 6915–6920.
(5) (a) Martinsen, J.; Greene, R. L.; Palmer, S. M.; Hoffman, B. M. *J. Am. Chem. Soc.* **1983**, *105*, 677–678. (b) Martinsen, J.; Palmer, S. M.; Tanaka, J.; Greene, R. L.; Hoffman, B. M. *Phys. Rev. B* **1984**, *30*, 6269–6276.
(6) Schramm, C. J.; Scaringe, R. P.; Stojakovic, D. R.; Hoffman, B. M.; Ibers, J. A.; Marks, T. J. *J. Am. Chem. Soc.* **1980**, *102*, 6702–6713.
(7) Barrett, P. A.; Linstead, R. P.; Tuey, G. A. P.; Robertson, J. M. *J. Chem. Soc.* **1939**, 1809–1820.

0020-1669/89/1328-3889$01.50/0

Table I. Crystal Data and Experimental Details for Cu(tatbp)I

formula	$C_{33}H_{17}CuIN_7$	μ, cm^{-1}	21.2
fw	702.00	transmission	0.912–0.943
a, Å	13.998 (5)	factors	
c, Å	6.426 (3)	R on F_o^2	0.085
V, Å^3	1259	R_w on F_o^2	0.109
Z	2	r on F_o, $F_o^2 >$	0.044
temp, K	120	$3\sigma(F_o^2)$	
d_{calc}, g/cm^3	1.851 (120 K)	R_w on F_o, $F_o^2 >$	0.086
space group	D_{4h}^2-$P4/mcc$	$3\sigma(F_o^2)$	
radiation, Å	λ(Mo Kα) = 0.7093		

carbon atom was prepared with the use of $^{13}CH_3I$ (Aldrich; >98%) in place of CH_3I. The crude product was purified by dissolution in concentrated sulfuric acid, filtration through sand, and precipitation over a mixture of NH_4OH and ice. The resultant material was sublimed three times prior to further use. Mass spectra were obtained on an HP5985 spectrometer by Dr. D. Hung of the Northwestern University Analytical Services Laboratory. The data are consistent with the formula $C_{33}H_{19}H_7$ and show no peaks attributable to phthalocyanine or the diaza ($C_{34}H_{20}N_6$) or monoaza ($C_{35}H_{21}N_5$) analogues of H_2(tatbp). Anal. Calcd for $C_{33}H_{19}N_7$: C, 77.2; H, 3.7; N, 19.1. Found, C, 77.3; H, 3.7; N, 19.0.

Cu(tatbp)I. (Triazatetrabenzoporphyrinato)copper(II), Cu(tatbp), was prepared by refluxing an excess of $CuCl_2$ with H_2(tatbp) in freshly distilled quinoline under a stream of nitrogen gas for several hours. The product was recrystallized from 1-chloronaphthalene and sublimed prior to use. Polycrystalline samples of Cu(tatbp)I were prepared by reacting solutions of Cu(tatbp) and I_2 in either 1,2,4-trichlorobenzene or 1-chloronaphthalene in an H-tube. The side containing the porphyrin was heated to 160 °C, and the reaction with I_2 occurred as the material diffused to the cold arm of the H-tube. Materials prepared at temperatures above 160 °C possessed different EPR line widths at temperatures above 100 K[8] but were otherwise indistinguishable from those prepared at 160 °C. Anal. Calcd for $C_{33}H_{17}CuI_{1.0}N_7$: C, 56.46; H, 2.44; N, 13.97. Found: C, 56.43; H, 2.45; N, 13.60.

X-ray Diffraction Study of Cu(tatbp)I. X-ray data from a single crystal of Cu(tatbp)I were collected on an Enraf-Nonius CAD4 diffractometer at 120 K. An initial search produced a tetragonal cell with parameters a = 13.998 (3) Å and c = 6.426 (3) Å, nearly identical with those of Cu(pc)I.[1] Intensity data were collected by the θ–2θ scan technique and were processed by methods standard in this laboratory.[9] No systematic change was observed in the intensities of six standard reflections measured ever 3 h of X-ray exposure time. Some experimental details are summarized in Table I; a more complete summary is in Table SI.[10] A total of 4609 reflections were observed. The data were corrected for absorption. Equivalent reflections (hkl, $\bar{h}kl$, $\bar{k}hl$, $\bar{k}\bar{h}l$, $h\bar{k}l$, $\bar{h}\bar{k}l$, khl, $k\bar{h}l$) were averaged, yielding 1002 unique data, of which 430 were found to have $F_o^2 > 3\sigma(F_o^2)$. Systematic absences were observed for reflections hhl and $0kl$ with l odd, consistent with the space group $P4/mcc$ or $P4cc$. A comparison with similar structures[1,4-6] and an agreement among averaged reflections (R of averaging 6.2%, including data with $F_o^2 \leq 0$) suggested that the structure is centrosymmetric. Successful refinement of the structure confirmed the choice of D_{4h}^2-$P4/mcc$ as the correct space group.

A Patterson map indicated that the positions of the iodine atoms are $\pm^1/_2$, $\pm^1/_2$, $\pm^1/_4$ away from the Cu atoms. A comparison with the known structures of similar compounds[1,4,6] and the added constraint that Z = 2 fixed the Cu atom on the site having symmetry $4/m$. All non-hydrogen atom positions were determined from subsequent electron density maps. The four bridging atoms of the tatbp unit lie on crystallographically equivalent sites. In each unit, however, three of these sites are occupied by N atoms and the fourth by a C atom. These four atoms were treated in the refinement as hybrids of N and C through the use of a weighted average of the individual scattering factors. Least-squares refinement on F_o with isotropic thermal parameters for all non-hydrogen atoms led to values of R and R_w of 0.11 and 0.13, respectively. When anisotropic thermal parameters were used, R and R_w decreased to 0.050 to 0.056, respectively. Hydrogen atom positions were located on a difference electron density map and their positions idealized (C–H = 0.95 Å) and not varied. Each H atom was assigned a thermal parameter 1 Å^2 greater than the C atom to which it is bonded. The hydrogen atom bonded to the methine carbon atom, however, is disordered among the bridge sites and was neither located nor idealized. The final refinement was carried out on F_o^2 and involved 65 variables and all 1002 unique data, including those with $F_o^2 < 0$. This refinement converged to the agreement indices given in Table I. Final positional and thermal parameters are given in Table II. Other crystallographic data will be found in the supplementary material.[10] Figure 1 depicts the Cu(tatbp) unit with the labeling scheme.

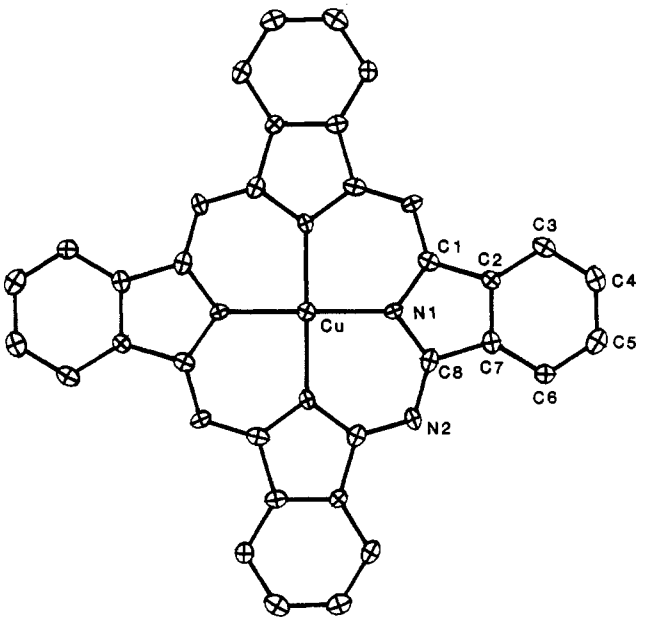

Figure 1. Drawing of Cu(tatbp)I with labeling scheme. Thermal ellipsoids are drawn at the 50% level. Hydrogen atoms have been omitted.

Physical Characterization. Raman spectra were obtained at ambient temperatures on polycrystalline samples of material contained in 5-mm Pyrex tubes as described earlier.[11]

Single crystals of Cu(tatbp)I were mounted on silvered graphite fibers (8 μm, Alfa/Ventron) for four-probe (27-Hz) ac conductivity measurement as described previously;[1] we treat these results as identical with those of dc measurements. Microwave conductivity measurements employed a standard microwave cavity perturbation technique.[3a] The typical dimensions of the sample used in the microwave experiment were 2 × 0.03 × 0.03 mm; the shape of the sample could be approximated with high accuracy by an elongated ellipsoid. The configuration of the experimental setup allowed measurements with the rf electrical field along the needle (c) axis of the sample and the external magnetic field in the transverse direction. Magnetic fields up to 7 T were produced by a Nb–Ti superconducting coil, while the temperature was monitored and stabilized by a Lakeshore controller with a $SrTiO_3$ capacitor. An overall precision of ±0.05 K was obtained over the 2–30 K temperature range.

Static magnetic susceptibility measurements were taken from 300 to 1.7 K with the use of a SHE VTS-50 SQUID susceptometer. Samples of polycrystalline material (ca. 30–40 mg) were crushed to avoid anisotropy effects and placed in holders made of high-purity Spectrosil quartz (Thermal American Inc.). The holder background was measured over the full temperature range just prior to each experiment. Calibration of the instrument was checked with a palladium standard obtained from the National Bureau of Standards. The measurements were performed at an external field of 10 kG.

A pulsed NMR spectrometer system[12] operating at 13 MHz (12.14 kG) was used to perform ^{13}C measurements on polycrystalline samples (ca. 200 mg) with ^{13}C in natural abundance (1% ^{13}C at the 33 carbon

(8) In attempting to perform a similar analysis for Cu(tatbp)I, we noticed that the high-temperature (T > 100 K) EPR line width properties of this material vary with preparation. We found that, depending on the particular sample studied, the line widths typically increase with decreasing temperature down to 100 K, in a manner similar to that observed for Cu(pc)I. However, in some cases they may decrease anomalously with decreasing temperature. In addition, those crystals displaying the latter behavior exhibited a somewhat broader EPR line, and we tentatively ascribe this unusual behavior to the previously observed, but not understood, "broad line" phenomena of Ni(pc)I. However, all other properties of Cu(tatbp)I, including the conductivity, magnetic susceptibility, high- and low-temperature EPR g-value behavior, and low-temperature (T < 100 K) line width behavior, remain independent of preparation.

(9) (a) Corfield, P. W. R.; Doedens, R. J.; Ibers, J. A. *Inorg. Chem.* **1967**, *6*, 197–204. (b) de Meulenaer, J.; Tompa, H. *Acta Crystallogr.* **1965**, *19*, 1014–1018.

(10) Supplementary material.

(11) Shriver, D. F.; Dunn, J. B. R. *Appl. Spectrosc.* **1974**, *28*, 319–323.

(12) Gibson, A. A. V.; Owers-Bradley, R., Jr.; Calder, I. D.; Ketterson, J. B.; Halperin, W. P. *Rev. Sci. Instrum.* **1981**, *52*, 1509–1516.

Table II. Positional Parameters and B_{eq} Values for Cu(tatbp)I

atom	x	y	z	B, Å²	atom	x	y	z	B, Å²
Cu	0	0	0	1.33 (2)	C(5)	0.44495 (45)	0.15392 (50)	0	2.2 (2)
I	1/2	1/2	1/4	3.08 (2)	C(6)	0.39059 (44)	0.07156 (43)	0	1.6 (2)
N(1)	0.12709 (32)	0.05978 (34)	0	1.1 (1)	C(7)	0.29169 (44)	0.08185 (43)	0	1.4 (2)
N(2)	0.08266 (37)	0.22815 (37)	0	1.2 (1)	C(8)	0.21370 (40)	0.01314 (48)	0	1.4 (2)
C(1)	0.14579 (46)	0.15640 (44)	0	1.4 (2)	H1C(3)	0.276	0.318	0	2.8
C(2)	0.24939 (45)	0.17169 (40)	0	1.3 (1)	H1C(4)	0.442	0.300	0	3.4
C(3)	0.30463 (47)	0.25472 (45)	0	1.8 (2)	H1C(5)	0.515	0.150	0	3.2
C(4)	0.40188 (47)	0.24370 (48)	0	2.2 (2)	H1C(6)	0.420	0.009	0	2.7

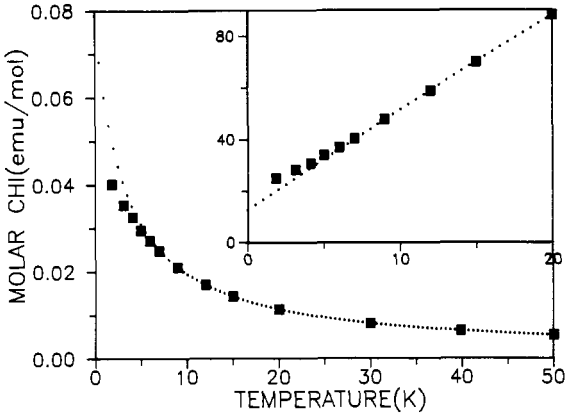

Figure 2. Static susceptibility of Cu(tatbp)I. The dotted line is a fit to eq 1; constants are given in the text. Inset: low-temperature data plotted as inverse susceptibility (mol emu^{-1}) versus temperature.

positions of tatbp) and with 90% ^{13}C enrichment at the methine carbon nucleus. Data were taken over the temperature range 4–50 K, with a $\pi/2$–π-echo pulse sequence.

EPR experiments at X-band frequencies (ca. 9 GHz) employed single crystals and methods standard to this laboratory[1] for temperatures down to $T \approx 5$ K. Lower temperatures employed powder samples and a pumped-helium immersion cryostat; similar samples and procedures were used for the Q-band-frequency (ca. 35 GHz) measurements.

Results

Resonance Raman Spectroscopy. The resonance Raman spectrum of polycrystalline Cu(tatbp)I at room temperature exhibits a sharp fundamental peak at 107 cm^{-1} with an overtone progression of peaks at 213, 320, and 436 cm^{-1}. This pattern is characteristic of linear chains of symmetrical triiodide ions.[13] The absence of any observable peaks having an intensity larger than that of the overtone band at either 167 or 212 cm^{-1} eliminates I_5^- or I_2 as the predominate iodine form in this material. By analogy with our study of Ni(pc)I,[6] for which ^{129}I Mössbauer experiments provided no evidence for the presence of I^-, we conclude that Cu(tatbp)I also contains no I^-. Thus, the proper formulation of Cu(tatbp)I is $[Cu(tatbp)I]^{0.33+}[I_3^-]_{0.33}$, indicating partial oxidation of 1/3 electron per metallomacrocycle.

Description of the Structure. As expected from similarities in unit cell constants, the structure of Cu(tatbp)I is essentially the same as that of Cu(pc)I.[1] It consists of columns of Cu(tatbp) metallomacrocycles segregated from chains of I_3^- anions. Each metallomacrocycle is on a site of $4/m$ symmetry and is constrained to be planar. The macrocycles stack metal over metal with their planes orthogonal to the stacking axis. The two macrocycles in the unit cell are rotated 39.6 (2)° with respect to one another. Chains of I_3^- anions lie in the channels between Cu(tatbp) stacks with each I atom on a site of 422 symmetry. The nature of the I_3^- arrangement has been discussed in detail for Ni(pc)I.[6] Each iodine chain is ordered along its length but disordered with respect to other I_3^- chains. This disorder gives rise to the abnormally high value for U_{33} for I. Bond distances and angles for Cu(tatbp)I are listed in Table III. All bond distances in Cu(tatbp)I agree with those in Cu(pc)I to within experimental error, except for a small increase in the M–N(1) distance of 0.031 (8) Å.

Table III. Selected Bond Distances (Å) and Angles (deg) for Cu(tatbp)I

bond	dist or angle	av[a]
Cu–N(1)	1.966 (5)	
N(1)–C(1)	1.378 (7)	
N(1)–C(8)	1.377 (7)	1.378 (7)
N(2)–C(1)	1.338 (7)	
N(2)–C(8)	1.356 (8)	1.346 (13)
C(1)–C(2)	1.466 (8)	
C(7)–C(8)	1.455 (8)	1.461 (8)
C(2)–C(7)	1.390 (8)	
C(2)–C(3)	1.396 (8)	
C(6)–C(7)	1.392 (8)	1.394 (8)
C(3)–C(4)	1.370 (8)	
C(5)–C(6)	1.381 (8)	1.376 (9)
C(4)–C(5)	1.394 (9)	
N(1)–Cu–N(1)	180	
Cu–N(1)–C(1)	126.1 (4)	
Cu–N(1)–C(8)	126.5 (4)	126.3 (4)
C(1)–N(1)–C(8)	107.4 (5)	
C(1)–N(2)–C(8)	122.8 (6)	
N(1)–C(1)–N(2)	127.7 (6)	
N(1)–C(8)–N(2)	126.9 (5)	127.2 (6)
N(1)–C(1)–C(2)	109.4 (5)	
N(1)–C(8)–C(7)	110.3 (6)	109.8 (6)
N(2)–C(1)–C(2)	123.0 (5)	
N(2)–C(8)–C(7)	122.8 (5)	122.9 (5)
C(1)–C(2)–C(3)	132.0 (5)	
C(6)–C(7)–C(8)	132.8 (6)	132.3 (6)
C(1)–C(2)–C(7)	106.8 (5)	
C(2)–C(7)–C(8)	106.3 (6)	106.6 (6)
C(3)–C(2)–C(7)	121.2 (6)	
C(6)–C(7)–C(2)	121.2 (6)	121.2 (6)
C(2)–C(3)–C(4)	117.2 (6)	
C(5)–C(6)–C(7)	117.5 (6)	117.4 (6)
C(3)–C(4)–C(5)	122.1 (6)	
C(4)–C(5)–C(6)	120.1 (6)	121 (1)

rotation angle between intrastack Cu(tatbp) molecules: 39.6 (2)

[a] Average values are weighted. The standard deviation given is the larger of that estimated for a single observation from the inverse matrix or on the assumption that the values averaged are from the same population.

Magnetic Susceptibility Measurements. Magnetic susceptibility measurements provide a convenient means of determining the nature of the charge carriers in Cu(tatbp)I. There are two limiting conditions. First, Cu(tatbp)I could exist as a metal-spine conductor similar to Co(pc)I.[4] In this case, partial oxidation of the paramagnetic Cu^{2+} sites would reduce the number of localized spins. Alternatively, partial oxidation from the organic ligand would leave the paramagnetic Cu^{2+} centers undisturbed. Cu(tatbp)I would then possess two distinct magnetic systems, a dense array of localized Cu^{2+} sites and a system of itinerant charge carriers; its magnetic susceptibility would have Curie-like contributions from the Cu^{2+} sites and an approximately temperature-independent Pauli-like term from the charge carriers. Such behavior has been observed for Cu(pc)I.[1]

Figure 2 presents the temperature dependence of the magnetic susceptibility of a polycrystalline sample of Cu(tatbp)I. To optimize characterization of the local spins, data were collected over the low-temperature range $2 \leq T \leq 50$ K. These are displayed in Figure 2 as χ^{-1} vs T to emphasize the predominately Curie–

(13) (a) Teitelbaum, R. C.; Ruby, S. L.; Marks, T. J. *J. Am. Chem. Soc.* **1978**, *100*, 3215–3217. (b) Teitelbaum, R. C.; Ruby, S. L.; Marks, T. J. *J. Am. Chem. Soc.* **1980**, *102*, 3322–3328.

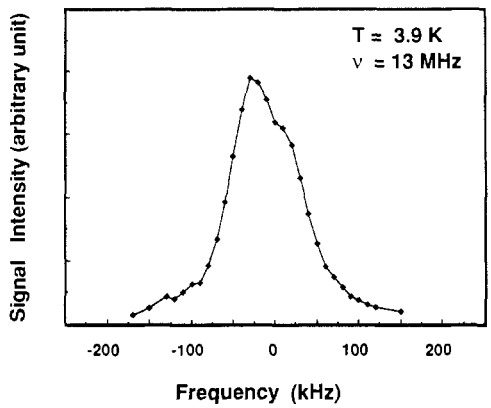

Figure 3. ^{13}C NMR spectrum of ^{13}C-enriched Cu(tatbp)I at 13 MHz and 3.9 K.

Weiss behavior evidenced by the nearly linear temperature dependence of the inverse susceptibility. The presence of an additional small, temperature-independent contribution to the susceptibility is indicated by a slight curvature of the plot at higher temperatures (not shown). The data taken in the 10–50 K range fit well to the expression

$$\chi(T) = \chi_{loc}(T) + \chi_{Pauli} = C/(T - \Theta) + \chi_{Pauli} \qquad (1)$$

where $\chi_{loc}(T)$ is the susceptibility of the localized spin system, expressed in a Curie–Weiss form, and χ_{Pauli} is the temperature-independent susceptibility of the charge carriers. The resulting parameters are $C = 0.428$ (9) emu K mol^{-1}, $\Theta = -6.9$ (3) K, and $\chi_\pi = 2.8$ (9) $\times 10^{-4}$ emu mol^{-1}, values similar to those observed for the related compound Cu(pc)I.[1] The Curie constant obtained from the fit is in good agreement with $C_0 = 0.406$ emu K mol^{-1} calculated for one Cu^{2+} spin per site

$$C_0 = S(S + 1)(Ng^2\beta^2/3k_B)$$

where N is Avogadro's number, β is the Bohr magneton, k_B is Boltzmann's constant, S is the electron spin, and $g^2 = 4.382$ is the average value for Cu^{2+} as discussed below. The Pauli susceptibility is similar to that observed for the macrocycle-based carriers of Ni(pc)I ($\chi_\pi = 2 \times 10^{-4}$ emu mol^{-1}).[5] These results indicate that Cu(tatbp)I is an organic conductor in which partial oxidation from the macrocyclic ligands creates a system of mobile charge carriers, leaving the one-dimensional array of localized Cu^{2+} spins (one per site) intact.

The susceptibility ceases to increase as rapidly as predicted by eq 1 when Cu(tatbp)I is cooled below $T \approx 6$–8 K (Figure 2). The temperature correlates with transitions in the EPR line width and microwave conductivity as discussed below.

^{13}C Nuclear Magnetic Resonance Spectroscopy. The ^{13}C NMR spectrum of methine-^{13}C Cu(tatbp)I is shown in Figure 3. The spectrum was taken by varying the frequency point by point and integrating the spin echo with a long pulse width. The same result is reproduced by a Fourier transform of the spin echo with a much narrower pulse. The spectrum is a composite of two peaks and narrows as the temperature is increased. The main peak comes from the enriched methine carbon nucleus; a shoulder on the high-frequency side of this absorption line is associated with naturally abundant ^{13}C nuclei distributed over 32 possible carbon sites in each molecular unit. This site assignment is confirmed by a ^{13}C spectrum of unenriched Cu(tatbp)I that shows the expected ratio of 3:1 for the two components of the line.

A negative frequency shift is observed for the enriched methine carbon nucleus and a positive shift for the distributed naturally abundant ^{13}C nuclei. Both shifts increase in magnitude as the temperature is lowered. The position of the shoulder on the main line in general cannot be measured accurately; its position was determined only at 3.9 K on unenriched Cu(tatbp)I. The two peaks shift roughly in proportion to the Cu^{2+} susceptibility (Figure 4). From the temperature dependence and magnitude of the shifts, it is clear that they are associated with electron spin density

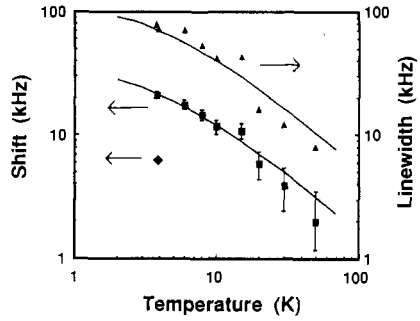

Figure 4. ^{13}C NMR frequency shift magnitudes (■) for the methine carbon nucleus of Cu(tatbp)I. The solid line is a fit to eq 2b; fitting parameters are $A = -0.39$ MHz and $\Theta = -4.1$ K. The line width for the total signal from the ^{13}C-enriched material also is presented (▲); the solid line connecting these points is only an aid to the eye in this case. A single point (♦) represents the magnitude of the average shift of the naturally abundant ^{13}C nuclei distributed over the 32 possible sites.

from the Cu local spin. One possible contribution is from a pseudocontact term.[14] This part of the shift[14] is

$$\frac{\Delta H}{H_0} \approx (g_\parallel^2 - g_\perp^2)\frac{\beta^2 S(S + 1)}{9k_B(T - \Theta)d^3} \qquad (2a)$$

where d is the distance from the Cu spin to the nucleus. Taking $d = 3.37$ Å as the distance to the methine carbon nucleus, we obtain a shift of ~2.6 kHz at 4 K, much smaller than observed. Another possible contribution to the frequency shift is from the isotropic part of the contact hyperfine interaction:[15]

$$\frac{\Delta H}{H_0} = -A\frac{g\beta}{[g(^{13}C)]\beta_N}\frac{S(S + 1)}{3k_B(T - \Theta)} \qquad (2b)$$

A fit of the data for the methine position of this equation gives $\Theta = -4.1$ K, in reasonable agreement with the static susceptibility measurements, and a hyperfine coupling constant of $A \cong -0.39$ (3) MHz.

The signs of the NMR shifts imply negative electron spin density at the enriched methine site and positive spin density averaged over naturally abundant sites. The value of A for the methine carbon nucleus corresponds to 0.01% of a spin in a 2s orbital. The line width, taken as the full width at half-maximum (fwhm) of the magnitude of the Fourier-transformed spectrum, broadens as the temperature is lowered in parallel with the increase in NMR frequency shifts (Figure 4), suggesting that a distribution of shifts determines the line width.

No unusual behavior is observed below 10 K from either shifts or line widths, a result consistent with the temperature dependence of the susceptibility. The spin–lattice relaxation time T_1 at the enriched site changes only from 40 to 45 ms as the temperature is lowered from 50 to 8 K. Because the spin–spin relaxation time T_2 (270–470 μs) $\ll T_1$, we believe that T_1 is dominated by slow electronic relaxation of Cu spins.[16] At temperatures $T \leq 8$ K, where the EPR line width broadens sharply, T_1 starts to decrease, reaching 34 ms at 4 K.

EPR g Values; $T > 20$ K. In the absence of exchange interactions between the local and itinerant spin systems, the EPR spectrum of Cu(tatbp)I would display two different resonances. The signal of the Cu^{2+} sites would have a **g** tensor similar to that found for Cu(pc) diluted into Ni(pc) ($g_\parallel = 2.187$; $g_\perp \approx 2.05$);[17] that associated with the oxidized macrocycles would exhibit a roughly isotropic **g** tensor ($g_\pi \approx 2.00$), as seen in Ni(pc)I.[5] Instead, strong exchange coupling ($J \gg (g_{Cu} - g_\pi)\beta H_0$) between the local and carrier spins in Cu(tatbp)I produces a single resonance with temperature-dependent g values. At all temperatures, the **g** tensor of Cu(tatbp)I is axially symmetric with the unique tensor axis

(14) McConnell, H. M.; Robertson, R. E. *J. Chem. Phys.* **1958**, *29*, 1361–1365.
(15) McConnell, H. M.; Chestnut, D. B. *J. Chem. Phys.* **1958**, *28*, 197–117.
(16) $\omega_M^2\tau^2 \gg 1$, where ω_M is the electron Larmor frequency and τ is the correlation time: Eaton, D. R.; Phillips, W. D. *Adv. Magn. Reson.* **1965**, *1*, 103–148.
(17) Harrison, S. E.; Assour, J. M. *J. Chem. Phys.* **1964**, *40*, 365–370.

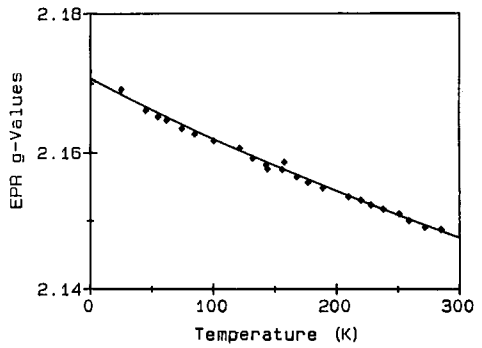

Figure 5. Parallel component of the EPR **g** tensor of a single crystal of Cu(tatbp)I taken as a function of temperature. The solid line is a fit to eq 3 as discussed in the text.

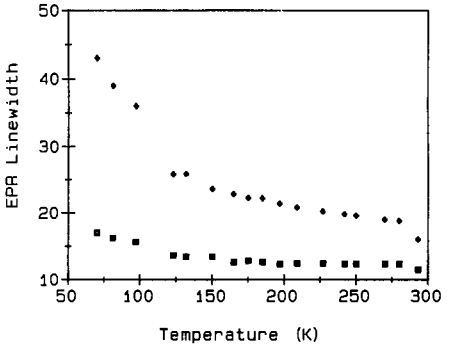

Figure 6. Parallel (♦) and perpendicular (■) components of the EPR derivative peak-to-peak line width of a single crystal of Cu(tatbp)I as a function of temperature.

corresponding to the (needle) c axis. At ambient temperatures, the principal components of the **g** tensor for a typical crystal of Cu(tatbp)I are $g_\parallel = 2.148$ and $g_\perp = 2.036$. These values are intermediate between those expected for isolated Cu(tatbp) and for π-carrier spins, and they further increase when the sample is cooled (Figure 5). This behavior is expected for the case of two exchange-coupled magnetic systems. Here the observed EPR g values occur at the susceptibility-weighted average of the individual component g values:[18,19]

$$g_{obs}(\theta,T) = f_{Cu}(T)\, g^{Cu}(\theta) + f_\pi g^\pi$$
$$\left.\begin{aligned} f_{Cu}(T) &= \chi_{Cu}(T)/(\chi_{Cu}(T) + \chi_\pi) \\ f_\pi(T) &= 1 - f_{Cu}(T) \end{aligned}\right\} \quad (3)$$

Here $g^{Cu}(\theta)$ is the angle-dependent g value of the one-dimensional array of Cu^{2+} spins, g^π is the isotropic g value of the π carriers, and $f(T)$ is the temperature-dependent fraction of the total Cu(tatbp)I susceptibility associated with the Cu^{2+} spins. Using the susceptibility results presented above to calculate $f(T)$ for Cu(tatbp)I, we have analyzed the parallel ($\theta = 0$) component of the **g** tensor for $T > 20$ K. Figure 5 shows good agreement between the observed EPR g values and the results of a nonlinear least-squares fit to eq 3 of the data at temperatures above ca. 25 K. The fit yields as the intrinsic g values of the individual spin components $g_\parallel^{Cu} = 2.171$ (1) and $g^\pi = 2.027$ (8). Thus, Cu(tatbp)I displays the strong local moment–itinerant spin coupling seen in Cu(pc)I. Note that no deviation from this fit occurs at temperatures $25 \le T \le 90$ K, where the conductivity of Cu(tatbp)I decreases sharply with temperature (see below). Thus, the decrease in the conductivity in this range cannot simply involve a localization of the π carriers that abolishes their Pauli paramagnetism, for this would cause f_{Cu} to become unity and $g_{obs}(\theta,T)$ to reach its limiting value, $g^{Cu}(\theta)$ (eq 3).

EPR Line Width Measurements: $T > 20$ K. Figure 6 presents the temperature dependence of the line width of the EPR signal of Cu(tatbp)I taken with the magnetic field parallel and perpendicular to the stacking axis. Because the signal is an exchange average of contributions from localized Cu^{2+} spins and itinerant carriers, the EPR line width of this material is the susceptibility-weighted average of the line widths of the local-moment and carrier spin systems[18]

$$\Delta_{obs} = f_\pi \Delta^\pi + f_{Cu}[\Delta^{Cu}(\theta)] \quad (4)$$

where f_π and f_{Cu} are the fractional susceptibilities defined in eq 3, Δ^π is the nearly isotropic line width of the π carriers, and Δ^{Cu} is the angle-dependent line width of the Cu^{2+} chain. Studies of one-dimensional Cu^{2+} complexes[20] show that the interplay of strong unidimensional dipolar and exchange interactions results in a narrowed EPR signal whose second moment has the angular dependence $M_2 \propto (1 + \cos^2\theta)$ when the exchange frequency ω_e exceeds the Larmor frequency. The form of the line width is $\Delta^{Cu} \propto (M_2/\omega_e) \propto (1 + \cos^2\theta)$. We therefore use the expression $\Delta^{Cu} = \Delta_D(1 + \cos^2\theta)$ in eq 4 to analyze the line width (derivative peak to peak) of the Cu^{2+} spins in Cu(tatbp)I at 293 K

$$\Delta(\theta) = f_\pi \Delta^\pi + f_{Cu}[\Delta_D(1 + \cos^2\theta)]$$
$$\equiv \Delta_0 + \Delta_1(1 + \cos^2\theta) \quad (5)$$

where the contribution of the angle-dependent term is set by the dipolar factor

$$\Delta_1 \equiv f_{Cu}\Delta_D \quad (6)$$

We tentatively assign the isotropic line width to the π-carrier spins $\Delta_0 = f_\pi \Delta_\pi$, although it may have other contributors as well. A nonlinear least-squares fit to eq 5 of the data taken at ambient temperatures is in good agreement with experiment and yields the values $\Delta_0 = 12.5$ (3) G and $\Delta_1 = 6.0$ (2) G.

Heuristic Model for EPR Line Width: $T > 20$ K. Analysis of the line width of Cu(tatbp)I further requires a description of the processes that narrow the dipolar line width of the copper spins. The dipolar interactions between local moments are modulated by exchange between copper centers,[20] the exchange frequency having contributions both from near-neighbor interactions caused by direct Cu–Cu overlap and from indirect, long-range (RKKY) interactions mediated through the itinerant carriers. In addition, studies of isolated local moments exchange-coupled to itinerant spins[18] suggest that one should also allow for a second, temperature-dependent contribution to ω_e arising from the dynamic exchange between local and itinerant moments: $\omega_x \propto T$. We therefore attempt to describe the modulation of the Cu^{2+} spins by an effective exchange frequency of the functional form

$$\hbar\omega_e \approx J + \hbar\omega_x \equiv k_B(a + bT) \quad (7)$$

Here, J represents the rms value at a site for the sum of the direct and indirect quantum-mechanical exchange coupling between copper centers; in a mean-field model the Weiss constant (eq 1) is $|\Theta| \approx a/2\sqrt{2}$. The second term, bT, represents the dynamical exchange between local and mobile spins. If this form is inserted into the expression for the dipolar line width in the strong exchange limit,[20] the dipolar factor Δ_D (eq 6) for a linear chain of Cu^{2+} spins becomes

$$\Delta_D = \frac{8}{3\sqrt{3}}\frac{m_D}{\hbar\omega_e} = \frac{8}{3\sqrt{3}}\frac{m_D}{k_B(a + bT)} \quad (8)$$

where

$$m_D = 3S(S+1)\frac{g^3\beta^3}{r^6}\sum_1^\infty n^{-6} = \frac{9}{4}\frac{(g\beta)^3}{r^6} \times 1.0173 \quad (9)$$

and $r = c/2 = 3.213$ Å is the Cu–Cu spacing and $S = {}^1/_2$. Values of Δ_1 (eq 5) have been calculated from the measured line widths (Figure 6) with the relation $\Delta_1 = \Delta_\parallel - \Delta_\perp$; Δ_D was calculated from Δ_1 from eq 6, and values of $f(T)$ (eq 3) were obtained from the susceptibility data. The roughly linear response of Δ_D^{-1} to tem-

(18) Barnes, S. E. *Adv. Phys.* **1981**, *30*, 801–938.
(19) (a) Alcacer, L., Maki, A. H. *J. Phys. Chem.* **1976**, *80*, 1912–1916. (b) Tomkiewicz, Y.; Taranko, A. R.; Torrance, J. B. *Phys. Rev. B* **1977**, *15*, 1017–1023. (c) Conwell, E. *Phys. Rev. B* **1980**, *22*, 3107–3112.
(20) (a) Soos, Z. G.; Huang, T. Z.; Valentine, J. S.; Hughes, R. C. *Phys. Rev. B* **1973**, *8*, 993–1002. (b) McGregor, K. T.; Soos, Z. G. *J. Chem. Phys.* **1976**, *64*, 2506–2517. (c) We take the near-neighbor exchange to have the form $(2J_0)\sum S_i S_{i+1}$. In this case the rms exchange is $J = 2\sqrt{2}J_0$: Smart, J. S. *Effective Field Theories of Magnetism*; W. B. Saunders: Philadelphia, 1966.

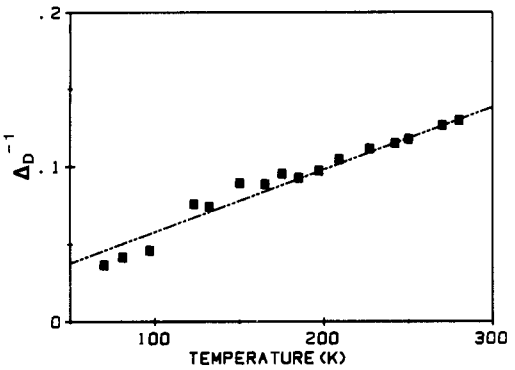

Figure 7. Inverse of the dipolar factor of the EPR line width Δ_D^{-1} (eq 8) of Cu(tatbp)I as a function of temperature. The dotted line represents the best fit of the data to eq 8.

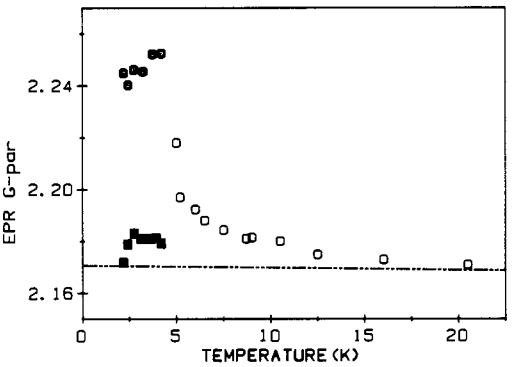

Figure 8. Low-temperature EPR g values: (○) single crystal; (●) polycrystalline sample at X-band; (■) polycrystalline sample at Q-band.

perature seen in Figure 7 is consistent with eq 8 and the assumed form of ω_e (eq 7); this supports the physical picture that leads to the model of the exchange interactions in Cu(tatbp)I. Values $J/k_B = a = 3.3$ K and $b = 7.6 \times 10^{-2}$ are obtained from a nonlinear least-squares analysis of the data of Figure 7, with the use of $m_D/k_B = 122$ G K, as calculated from eq 9. Note that this analysis suggests that for $T \gtrsim 40$ K the dynamical contribution dominates ω_e, but by $T \approx 20$ K it is less than half the Cu–Cu exchange term J. We consider the fact that the Weiss constant Θ determined from the susceptibility data does not agree well with a mean-field value obtained from J to be less important than the clear indication that ω_e is temperature-dependent.

Low-Temperature EPR Measurements; X-Band. As shown in Figure 8, the EPR g values of Cu(tatbp)I follow the susceptibility-weighted average of the two coupled spin systems (eq 3) from ambient temperature down to $T_a \approx 20$ K. Below ~20 K, $g_\parallel$ increases dramatically above the predictions of eq 3. By $T \approx 4.0$ K, $g_\parallel$ reaches a maximum of ~2.255, far greater than the value 2.171 extrapolated from the high-temperature regime. As the temperature is lowered further to $T \approx 2.4$ K, $g_\parallel$ decreases slightly.

The EPR line width, which increases as the temperature is lowered to T_a, does not broaden significantly and in fact decreases slightly (Figure 9) as T is lowered below T_a to $T_b \approx 6$–8 K. Thus, for $T_b < T < T_a$ the temperature variation of ω_e must cease; the value $\hbar\omega_e/k_B \approx 3$ K cannot diminish significantly between 20 and 8 K, or else the line width would increase (eq 5 and 6). At T_b the line width begins to increase dramatically. This second anomaly occurs, within error, at the temperature of the analogous line-broadening anomaly in Cu(pc)I. However, the EPR signal of Cu(pc)I broadens to the point of disappearance within a range of ±1 K around T_b, whereas the signal of Cu(tatbp)I remains observable and continues to broaden down to temperatures as low as 1.9 K.

Q-Band EPR Measurements. Prompted by the magnetoresistance measurements described below, we performed EPR measurements at a higher magnetic field (Q-band frequency, 35 GHz). The g values at convenient selected temperatures in the high-

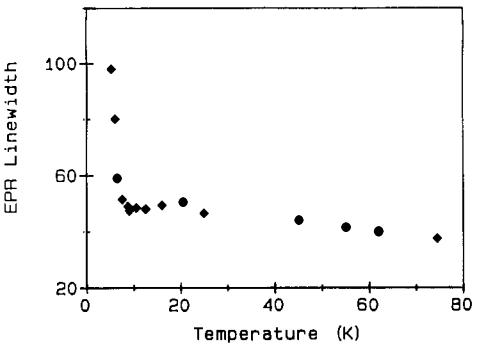

Figure 9. Low-temperature EPR line width (G) of Cu(tatbp)I ($H_0 \| c$).

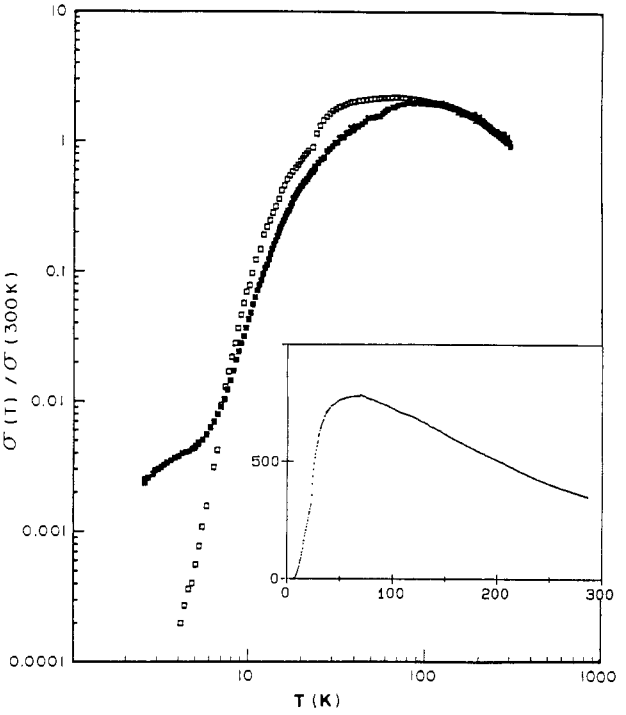

Figure 10. Normalized conductivity $\sigma(T)/\sigma(300\text{ K})$ of Cu(tatbp)I taken along its stacking axis as a function of temperature: (□) four-probe at 27 Hz; (■) microwave at 13 GHz. Inset: four-probe single-crystal conductivity (Ω^{-1} cm^{-1}).

temperature regime (270, 100 K) match those measured at X-band frequency. However, in the low-temperature regime they are not the same. As illustrated in Figure 8, at 4.2 K $g_\parallel(X) \approx 2.255$, whereas $g_\parallel(Q) \approx 2.18$; the Q-band value is roughly constant from ambient temperature to $T \approx 2.3$ K, although it may be decreasing slightly. Thus, the anomalous g shift seen at X-band frequency is quenched at higher observing field and the electronic structure itself, as reflected in $g_\parallel$, is a function of the applied field. The shapes of the $g_\parallel$ temperature dependences for X-band and Q-band measurements suggest that they would converge in the vicinity of T_b.

Four-Probe and Microwave Conductivity Measurements. Single crystals of Cu(tatbp)I exhibit four-probe (27-Hz) conductivity in the range 100–500 Ω^{-1} cm^{-1} at ambient temperatures. The fragility of these crystals makes low-temperature measurements difficult. Results from approximately 20 crystals show that the conductivity of Cu(tatbp)I increases with decreasing temperature in a metallic fashion ($d\sigma/dT < 0$) from ambient temperature to 150 K, where most samples broke. However, the conductivity of a few crystals of Cu(tatbp)I has been successfully measured throughout the entire temperature range $290 \geq T \geq 5$ K (Figure 10, inset). The crystals show a conductivity maximum ($\sigma_{max}/\sigma_{RT} = 1.8$) at approximately 90 K, followed by a rapid decrease in σ as the temperature is lowered toward 5 K.

In Figure 10 we compare the normalized conductivity $\sigma(T)/\sigma(300\text{ K})$ deduced from the microwave data[3] at 13 GHz with the four-probe measurements. The two curves agree well from am-

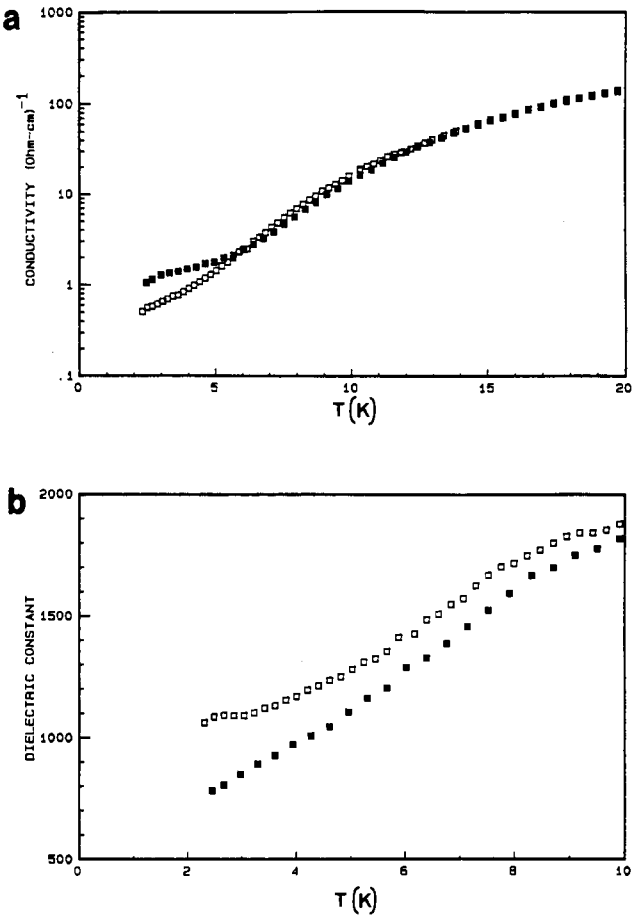

Figure 11. Temperature dependence of the single-crystal microwave conductivity of Cu(tatbp)I (a) and the dielectric constant (b) at 13 GHz: (■) $B = 0$; (□) $B = 7$ T.

bient temperature to ~10 K, indicating that the maximum at ~90 K is an intrinsic property and is not caused by strains from the contacts. Significant discrepancy between the two curves is observed for temperatures below 10 K: for $T < 6$ K, approximately the transition temperature seen in the EPR measurements, the microwave conductivity is *enhanced* in comparison to the four-probe conductivity.

The microwave conductivity (Figure 11a) and the dielectric constant (Figure 11b) were obtained as a function of temperature for magnetic fields up to 7 T. The largest magnetic field effects are seen for $T < 6$ K, and the curves in Figure 11a intersect at $T \simeq 6$ K, which separates two distinct regimes. Below 6 K the conductivity decreases significantly when the magnetic field is applied, whereas it increases slightly with field at higher temperatures. Figure 11b shows that the dielectric constant is an increasing function of the temperature over the range where it can effectively be measured (low conductivity) and that it increases with magnetic field.

Discussion

The results presented here and previously[1] show that Cu(pc)I and Cu(tatbp)I are isostructural molecular metals that contain a dense, one-dimensional array of local Cu^{2+} moments strongly coupled by a temperature-dependent exchange interaction and further exchange-coupled to the itinerant charge carriers associated with the π molecular orbitals of the ring. The mechanism for this coupling most likely involves Cu^{2+} spin density that is shown by the ^{13}C NMR data to be present on the macrocycle.

In both materials this unusual situation produces several transitions in the magnetic properties: at $T_a \approx 20$ K the g values and, to a lesser extent, the line widths begin to deviate from the high-temperature behavior; at $T_b \approx 6$–8 K there is a dramatic transition in the line width.[1] However, this second transition is substantially different in Cu(pc)I and Cu(tatbp)I. In Cu(pc)I the transition is characterized by a sudden broadening and disappearance of the EPR signal within ~1 K without an associated loss of paramagnetism, whereas in Cu(tatbp)I the signal remains observable below 8 K and the g value and line width continue to increase as the temperature is decreased. At X-band frequency, $g_\parallel$ of Cu(tatbp)I reaches a maximum of ~2.255 at 4 K and then decreases slightly. The increase in g value from ~20 to ~4 K cannot *simply* reflect uncoupling of the local moments from the itinerant spins: the maximum $g_\parallel$ is substantially greater than that for Cu(tatbp) itself.

In the temperature range below T_b, $g_\parallel^{Cu}$ itself is a function of applied field, with the anomalously large g shift being quenched at Q-band frequency. This suggests that the transition(s) seen in Cu(tatbp)I, and by inference in Cu(pc)I, cannot be assigned to a spin-Peierls (SP) transition.[21] The X-band EPR signal disappears at temperatures below such a transition and reappears with anomalous g shifts at very high observing fields. This contrasts with the quenching of the unusual X-band g shifts of Cu(tatbp)I when the observing field is increased from ~0.3 T (X-band) to ~1.2 T (Q-band).

The charge transport of Cu(tatbp)I is metallic from ambient temperature to ca. 90 K; below this the conductivity decreases in both microwave and four-probe measurements. It is very tempting to associate the conductivity data with paramagnetic scattering, namely an independent Kondo impurity model.[22-24] As the temperature is reduced, the Cu^{2+} local moments will act as scattering centers for the free carriers and the conductivity maximum observed at 90 K as well as the rapid falloff of 3 orders of magnitude may result from such a scattering process. In the limit of independent spins, an external magnetic field should partially freeze the local moments and thus reduce the scattering rate of the itinerant carriers; a positive magnetoconductivity is then expected.[21] The small positive magnetoconductivity over a temperature range that corresponds to $T_b \leq T \leq T_a$ is consistent with this magnetic scattering picture. Similar effects have also been observed in Cu_xNi_{1-x}(pc)I alloys.[25] However, in a three-dimensional independent Kondo impurity system, the overall variation of the conductivity is only 10% and the temperature dependence is logarithmic.[24] For our results no logarithmic tail is observed and the variation is over 3 orders of magnitude; this large variation might be attributed to the low dimensionality of the compound as scattering effects and localization are expected to be more dramatic in one dimension. It could be that Cu(tatbp)I is a rare example of a one-dimensional Kondo *lattice* system, because the EPR measurements reveal a strong coupling between the Cu^{2+} local moments and the free carriers. However, no calculation of the conductivity has been reported in the literature for such a system and we thus retain at present the independent Kondo impurity picture.

In the lower temperature range, $T \leq 6$ K, the enhancement of the conductivity at microwave frequency might result from dielectric losses. The onset of these proposed losses correlates well with the sudden increase of the EPR line width at T_b. This suggests that both phenomena reflect the opening of a new relaxation channel for the local moments. This new relaxation is blocked by the application of an external magnetic field; a strong field causes a decrease of the effective conductivity, presumably because the component arising from dielectric losses is quenched, and also causes an increase of the dielectric constant (real part). The mechanism that produces the dielectric losses is not yet understood, but its presence would imply an intriguing coupling

(21) Hijmans, T. W.; Beyermann, W. P. *Phys. Rev. Lett.* **1987**, *58*, 2351–2354.
(22) Kondo, J. *Solid State Phys.* **1969**, *23*, 183–281.
(23) Heeger, A. J. *Solid State Phys.* **1969**, *23*, 283–411.
(24) Van Den Berg, G. J. *Prog. Low Temp. Phys.* **1964**, *4*, 194.
(25) Ogawa, M. Y.; Palmer, S. M.; Liou, K. K.; Quirion, G.; Poirier, M.; Hoffman, B. M. *Phys. Rev. B* **1989**, *39*, 10682–10692. These results on Cu_xNi_{1-x}(pc)I alloys and the strong published evidence that the ring-oxidized M(L)I species behave as "simple" band-type (small-U) one-dimensional metals,[1,5] as well as unpublished thermopower measurements on Cu(tatbp)I, all show that the transport results on Cu(tatbp)I are not to be interpreted by analogy with those for certain TCNQ salts[26] because the latter materials are large-U Peierls systems.

between magnetic and dielectric properties. To pursue the investigation of the two distinct conductivity regimes observed in this type of conductor, we have initiated measurements of the microwave properties of alloy samples of the form $Cu_xNi_{1-x}(L)I$, where L = pc and tatbp.[25] In these materials a fraction of the copper ions is replaced by nickel ions that do not possess a local moment, which allows us to follow the effects of the concentration of local moments on both conductivity and dielectric losses.[26]

(26) Jawadi, H. H. S.; Miller, J. S.; Epstein, A. J. *Phys. Rev. Lett.* **1987**, *59*, 1760-1763.

Acknowledgment. This work has been supported by the Solid State Chemistry Program of the National Science Foundation (Grant DMF-8818599; B.M.H.), by the Northwestern University Materials Research Center under the NSF-MRL program (Grant DMF-8821571; W.P.H., B.M.H. and J.A.I.), and by the NSERC and FCAR (M.P).

Supplementary Material Available: Crystallographic details (Table SI) and anisotropic thermal parameters (Table SII) (3 pages); $10|F_c|$ vs $10|F_o|$ (Table SIII) (5 pages). Ordering information is given on any current masthead page.

Contribution from the Department of Chemistry, University of Wisconsin—Madison, Madison, Wisconsin 53706

Structural, Optical, and Redox Properties of Lamellar Solids Derived from Copper(I) Complexes and *n*-Butylammonium Uranyl Phosphate and Arsenate

Anthony T. Jacob and Arthur B. Ellis*

Received February 8, 1989

A family of hydrated, layered solids has been prepared from intercalative ion-exchange reactions of *n*-butylammonium uranyl phosphate (BAUP) or arsenate (BAUAs), $(n\text{-}C_4H_9NH_3)UO_2EO_4\cdot 3H_2O$ (E = P, As), with $Cu(LL)_2^+$ complexes (LL is dmp = 2,9-dimethyl-1,10-phenanthroline or bcp = 2,9-dimethyl-4,7-diphenyl-1,10-phenanthroline). The products obtained were analyzed as having compositions $[Cu(LL)_2]_x[BA]_{1-x}UO_2EO_4\cdot 2H_2O$ with $x \sim 0.2$. X-ray powder diffraction data reveal that the compounds are single phases that can be indexed on the basis of a tetragonal unit cell. The solids exhibit absorption and photoluminescence (PL) properties characteristic of the $Cu(LL)_2^+$ species; the Cu(I) complexes completely quench the uranyl PL. Once intercalated, the Cu(I) complexes can be oxidized by using Br_2 vapor and rereduced either by photochemical means or by N_2H_4 vapor, as shown by changes in electronic and EPR spectra.

Introduction

Layered phosphates and arsenates are proving to be versatile host lattices for intercalative ion-exchange reactions.[1] We and others have shown that a variety of transition-metal complexes can be intercalated into such hosts as $\alpha\text{-}Zr(HPO_4)_2$ (ZrP), $HUO_2PO_4\cdot 4H_2O$ (HUP), $HUO_2AsO_4\cdot 4H_2O$ (HUAs), $(n\text{-}C_4H_9NH_3)UO_2PO_4\cdot 3H_2O$ (BAUP), and $(n\text{-}C_4H_9NH_3)\text{-}UO_2AsO_4\cdot 3H_2O$ (BAUAs).[2-9] The intercalants have participated in a variety of reactions, including excited-state energy transfer,[2] ligand photosubstitution,[4] and acid-base/precipitation chemistry.[5]

An appealing set of candidate intercalants are Cu(I) complexes with bidentate ligands, $Cu(LL)_2^+$. In particular, the room-temperature photoluminescence (PL) and redox activity of the complexes $Cu(dmp)_2^+$ and $Cu(bcp)_2^+$ (dmp = 2,9-dimethyl-1,10-phenanthroline; bcp = 2,9-dimethyl-4,7-diphenyl-1,10-phenanthroline) have permitted extensive characterization of ground- and excited-state reactivity.[10-16] We sought to determine how these properties would be influenced by incorporation of the complexes into suitable lamellar host solids.

We report in this paper that single-phase, hydrated, lamellar solids of approximate composition $[Cu(LL)_2]_x\text{-}[BA]_{1-x}UO_2EO_4\cdot 2H_2O$ (E = P, As; BA = *n*-butylammonium; $x \sim 0.2$) can be prepared by intercalative ion-exchange reactions of the Cu(I) complexes with BAUP and BAUAs. Optical measurements reveal that while the photophysical properties of the Cu(I) complexes remain largely intact upon intercalation, strong host-guest interactions occur: the Cu(I) complexes quench the host UO_2^{2+} PL. We also demonstrate that the Cu(I) complexes undergo reversible redox chemistry that parallels their solution reactivity.

Experimental Section

Materials. Reagent grade $CuSO_4\cdot 5H_2O$ was supplied by Matheson Coleman and Bell; 2,9-dimethyl-1,10-phenanthroline ("neocuproine"; 98%), 2,9-dimethyl-4,7-diphenyl-1,10-phenanthroline ("bathocuproine"; 99%), L-ascorbic acid (99%), and hydrazine monohydrate (98%) were supplied by Aldrich; reagent grade bromine was supplied by J. T. Baker; analytical grade $UO_2(NO_3)_2\cdot 6H_2O$ and H_3PO_4 (85%) were supplied by Mallinckrodt; and As_2O_5 (99.9%) was supplied by Cerac. All materials were used as received. A 1.0 M solution of H_3AsO_4 was prepared by dissolving 11.5 g of As_2O_5 into 100 mL of boiling, triply distilled water. HUAs and HUP were prepared from uranyl nitrate and arsenic and phosphoric acid, respectively, as previously described.[3,17] BAUAs and BAUP were prepared from reactions of *n*-butylamine with HUAs and HUP, respectively, as described previously.[18]

For the intercalants prepared below, Cu analyses were conducted by ICP emission spectroscopy using a Leeman Laboratories ICP 2.5 inductively coupled plasma emission spectrophotometer. Compounds were dissolved in a minimum amount of concentrated HCl/HNO_3, followed by dilution with deionized water. Standardized solutions for the ICP analyses were prepared by dissolving copper wire (Malin Co.) in a min-

* To whom correspondence should be addressed.

(1) Clearfield, A. *Chem. Rev.* **1988**, *88*, 125.
(2) Olken, M. M.; Verschoor, C. M.; Ellis, A. B. *Inorg. Chem.* **1986**, *25*, 80.
(3) Olken, M. M.; Biagioni, R. N.; Ellis, A. B. *Inorg. Chem.* **1983**, *22*, 4128.
(4) Olken, M. M.; Ellis, A. B. *J. Am. Chem. Soc.* **1984**, *106*, 7468.
(5) Dieckmann, G. H.; Ellis, A. B. *Inorg. Chem.* **1987**, *26*, 4147.
(6) Ferragina, C.; Massucci, M. A.; Patrono, P.; Tomlinson, A. A. G.; La Ginestra, A. *Mater. Res. Bull.* **1987**, *22*, 29.
(7) Ferragina, C.; Massucci, M.; Patrono, P. *J. Chem. Soc., Dalton Trans.* **1988**, 851.
(8) Ferragina, C.; Massucci, M.; Patrono, P.; La Ginestra, A.; Tomlinson, A. A. G. *J. Chem. Soc., Dalton Trans.* **1986**, 265.
(9) Olken, M. M.; Verschoor, C. M.; Ellis, A. B. *J. Lumin.* **1984**, *31 & 32*, 552.
(10) Goodwin, K. V.; McMillin, D. R. *Inorg. Chem.* **1987**, *26*, 875.
(11) Goldstein, S.; Czapski, G. *Inorg. Chem.* **1985**, *24*, 1087.
(12) Kirchhoff, J. R.; Gamache, R. E., Jr.; Blaskie, M. W.; Del Paggio, A. A.; Lengel, R. K.; McMillin, D. R. *Inorg. Chem.* **1983**, *22*, 2380.
(13) Davies, K. M. *Inorg. Chem.* **1983**, *22*, 615.
(14) Holwerda, R. A. *Inorg. Chem.* **1982**, *21*, 2107.
(15) Blaskie, M. W.; McMillin, D. R. *Inorg. Chem.* **1980**, *19*, 3519.
(16) Ahn, B.; McMillin, D. R. *Inorg. Chem.* **1978**, *17*, 2253.
(17) Weigel, F.; Hoffmann, G. *J. Less-Common Met.* **1976**, *44*, 99.
(18) Pozas-Tormo, R.; Moreno-Real, L.; Martinez-Lara, M.; Bruque-Gamez, S. *Can. J. Chem.* **1986**, *64*, 30.

0020-1669/89/1328-3896$01.50/0